International Journal of Automation and Computing
www.ijac.net

18(5), October 2021, 802-813
DOI: 10.1007/s11633-021-1282-3

Robust Optimal Higher-order-observer-based Dynamic Sliding Mode Control for VTOL Unmanned Aerial Vehicles

Yashar Mousavi[1] Amin Zarei[2] Arash Mousavi[3] Mohsen Biari[4]

[1]Department of Applied Science, School of Computing, Engineering and Built Environment, Glasgow Caledonian University, Glasgow G4 0BA, UK

[2]Department of Electrical and Computer Engineering, University of Sistan and Baluchestan, Zahedan 9816745845, Iran

[3]Department Electrical Engineering and Applied Sciences, Paradise Research Center, Jahrom 7416813647, Iran

[4]Faculty of Electrical and Robotic Engineering, Shahrood University of Technology, Shahrood 3619995161, Iran

Abstract: This paper investigates the precise trajectory tracking of unmanned aerial vehicles (UAV) capable of vertical take-off and landing (VTOL) subjected to external disturbances. For this reason, a robust higher-order-observer-based dynamic sliding mode controller (HOB-DSMC) is developed and optimized using the fractional-order firefly algorithm (FOFA). In the proposed scheme, the sliding surface is defined as a function of output variables, and the higher-order observer is utilized to estimate the unmeasured variables, which effectively alleviate the undesirable effects of the chattering phenomenon. A neighboring point close to the sliding surface is considered, and as the tracking error approaches this point, the second control is activated to reduce the control input. The stability analysis of the closed-loop system is studied based on Lyapunov stability theorem. For a better study of the proposed scheme, various trajectory tracking tests are provided, where accurate tracking and strong robustness can be simultaneously ensured. Comparative simulation results validate the proposed control strategy′s effectiveness and its superiorities over conventional sliding mode controller (SMC) and integral SMC approaches.

Keywords: Unmanned aerial vehicle, dynamic sliding mode, trajectory tracking, fractional firefly algorithm, vertical take-off and landing system.

Citation: Y. Mousavi, A. Zarei, A. Mousavi, M. Biari. Robust optimal higher-order-observer-based dynamic sliding mode control for VTOL unmanned aerial vehicles. *International Journal of Automation and Computing*, vol.18, no.5, pp.802–813, 2021. http://doi.org/10.1007/s11633-021-1282-3

1 Introduction

In recent years, unmanned aerial vehicles (UAVs) with vertical take-off and landing (VTOL) maneuverability have received considerable attention due to their capacities of hovering and low-speed/low-altitude flight[1], and potential applications in agriculture, structures or oil pipelines inspection, law enforcement, sports, surveillance, mining, fire and traffic monitoring, and aerial imaging. These underactuated vehicles are canonical nonlinear systems with a three degrees of freedom mechanism and only two actuators, and the translational motion is controlled by a thrust force along a single body-fixed axis[2]. Moreover, VTOLs are members of a class of systems that cannot be fully controlled, i.e., some degrees of freedom cannot be directly controlled. Consequently, many strategies developed for fully controlled systems are not suitable and applicable to these systems. The existence of different characteristics in UAVs has generated a number of technical problems for control engineers. Accordingly, they can be considered as a benchmark for developing mathematical techniques to control actual unmanned flying devices.

Control of non-minimum phase nonlinear VTOL UAVs is a challenging problem in aerospace engineering, and several methodologies, including position stabilization and trajectory tracking for UAVs in the presence of external disturbances, have been investigated in the literature to deal with this problem[3–10]. However, many of these studies fail to deal with the control performance and robustness issues simultaneously. Although some controllers allow acceptable set-point tracking performance, the disturbance rejection issue has been found to be more significant for many others. Thus, designing a control strategy that emphasizes disturbance rejection with good set-point tracking is a real design problem that this work will focus on.

In [3], a new control strategy was proposed and formulated using an approximated solution for the tracking

Research Article
Manuscript received September 27, 2020; accepted January 22, 2021; published online March 20, 2021
Recommended by Associate Editor Min Tan
Colored figures are available in the online version at https://link.springer.com/journal/11633

problem in the basin of the linear algebra. In addition, some control strategies were successfully developed to guarantee global asymptotic stability[4–6]. A number of feedback control designs and various operating modes encountered in practice are studied for VTOL UAVs[7]. Based on the dynamic communication network and distributed robust feedback control approach, formation and reconfiguration control and collision avoidance of a team of VTOL UAVs can be analyzed. An inner-outer loop trajectory tracking feedback controller for a class of underactuated VTOL UAVs was developed in [8]. As the authors reported, the proposed paradigm demonstrated a remarkable performance through position and attitude tracking in the presence of uncertainties and exogenous disturbances. A centralized predictive interaction control scheme was investigated in [9] to deal with the ceiling effort problem of VTOL UAVs. According to the authors, the system's aerodynamic parameters were identified in real-time, where experimental investigations demonstrated the superior performance of the proposed strategy compared with the proportional-integral-derivative controller. Bouzid et al.[10] proposed a novel nonlinear internal model control scheme for trajectory tracking of a VTOL multi-rotors UAV under structured and unstructured disturbances. The coordinated trajectory tracking of multiple VTOL UAVs to drive all follower VTOL UAVs and to track the desired trajectory associated with a leader accurately based on defining novel distributed estimators is investigated in [11, 12]. Image-based tracking control algorithms were studied for VTOL UAVs to track a moving target[13, 14], which incorporated estimations of the target's acceleration without linear velocity measurements. Nevertheless, the position and orientation dynamics control problem was carried out by linear velocity estimations and the gravitational inertial direction extracted from image features[15]. Sliding modes-based methodologies for the planar VTOL (PVTOL) system were presented in [16, 17]. In addition, a two-step output-feedback control strategy was presented in [18] for regulation of a planar VTOL aircraft, such that the first controller stabilized the vertical variable based on an augmentation of a terminal sliding mode controller and a simple feedback linearization procedure, while the second controller stabilized the horizontal and angular variables using an energy-control method.

The firefly algorithm (FA) is a metaheuristic algorithm inspired by nature and has been successfully utilized for solving optimization problems[19]. Although FA has proved its exceptional advantages in comparison with other evolutionary algorithms, it has some shortcomings, such as inability to make a reasonable trade-off between exploration and exploitation behaviors, and suffering from getting trapped into local minima, significantly when solving complex multimodal problems[20, 21]. To overcome these drawbacks, various modifications have been investigated[22–25]. One of the most recent well-performed modifications of FA introduced in the literature is the fractional-order FA (FOFA), which incorporates the fractional calculus concepts into FA's search process. Since the performance of fractional-based optimization algorithms has been well-proven in [24, 26], FOFA will be utilized in this study for performance enhancement of the proposed control strategy.

Sliding mode control (SMC) has been utilized as one of the most efficient control approaches to deal with nonlinear systems subjected to external disturbances[27–30], however, it suffers from the chattering phenomenon[31–33]. To alleviate the chattering problem arising from the switching control action, a dynamic sliding mode control (DSMC) technique as a member of the variable structure controllers' family was investigated for nonlinear systems[34]. One contribution of this paper is to develop an optimal dynamical sliding mode control to deal with the VTOL position trajectory tracking control problem subjected to parametric uncertainties and external disturbances. A higher-order sliding mode observer (HSMO) is utilized to estimate the unmeasured variables in order to enhance the controllers′ performance with respect to chattering effects. Besides, the sliding surface is defined as a function of output variables, as a virtual output, which effectively reduces the undesirable properties of classical sliding mode such as the chattering phenomenon. To this end, a robust variable-structure control law is applied so that a neighboring point near the sliding surface is considered; and when the tracking error reaches to this point, the second control is activated and exponentially reduces the control signal. An output regulation scheme is employed on the state-space model of nonlinear time-variable systems in the present work. As a result, the proposed control strategy sets the output regulation error to the least possible value, while the states and input remain limited. To better illustrate the proposed control strategy's effectiveness and performance, it is applied to various reference trajectories.

The rest of this paper is organized as follows. In Section 2, the problem and some useful preliminaries are provided. In Section 3, the proposed control scheme and stability analysis are stated. Simulation results are provided in Section 4 to verify the theoretical results. Finally, conclusions are presented in Section 5.

2 Preliminaries

2.1 Fractional-order firefly algorithm

In FA, the swarm of fireflies moves toward more attractive and brighter fireflies. The attractiveness directly relates to the flashing light intensity associated with the objective function to be optimized. The relation between light intensity I_l and the distance r is expressed as

$$I_l = I_{l,0}\mathrm{e}^{-\gamma r} \tag{1}$$

where I_0 and γ denote the initial light intensity and the light absorption coefficient, respectively. The firefly's attractiveness β of firefly can be expressed as

$$\beta_r = \beta_0 \mathrm{e}^{-\gamma r} \tag{2}$$

where β_0 is the attractiveness at $r = 0$. According to [24], the movement of a firefly i attracted to another more attractive firefly j is calculated by

$$\mathfrak{D}^{\Omega}\left[x_{t+1}\right] = \beta_r\left(x_j - x_i\right) + \eta(\psi - 0.5) \tag{3}$$

where $\mathfrak{D}^{\Omega}[x(t)]$ denotes the Grünwald–Letnikov discrete-time fractional differential operator expressed as

$$\mathfrak{D}^{\Omega}[x(t)] = \frac{1}{T^{\Omega}} \sum_{q=0}^{z} \frac{(-1)^q \Gamma(\Omega+1) x(t-qT)}{\Gamma(q+1)\Gamma(\Omega-q+1)} \tag{4}$$

where $T = \Omega = 1$, and z is the truncation order. According to (3) and the first $z = 4$ terms of differential derivative, the following result obtains[24]:

$$\begin{aligned} x(t+1) = {} & \Omega x(t) + \beta_r\left(x_j - x_i\right) + \eta(\psi - 0.5) + \\ & \frac{1}{2!}\Omega(1-\Omega)x(t-1) + \frac{1}{3!}\Omega(1-\Omega)\left(2-\Omega\right)x(t-2) + \\ & \frac{1}{4!}\Omega(1-\Omega)(2-\Omega)\left(3-\Omega\right)x(t-3). \end{aligned} \tag{5}$$

2.2 VTOL modeling

The dynamic equations of motion have been described as (6)[35]. Also, Fig. 1 shows the normalized equations of the VTOL.

$$\begin{aligned} \ddot{x}(t) &= -u_1(t)\sin\theta(t) + \tau u_2(t)\cos\theta(t) + \psi_1(t) \\ \ddot{y}(t) &= u_1(t)\cos\theta(t) + \tau u_2(t)\sin\theta(t) - 1 + \psi_2(t) \\ \ddot{\theta}(t) &= u_2(t) \end{aligned} \tag{6}$$

where $x(t)$ and $y(t)$ are the center of mass horizontal and vertical positions, respectively. θ represents the angle concerning the imaginary horizontal line, $u_1(t)$ and $u_2(t)$ respectively represent the thrust force that causes the

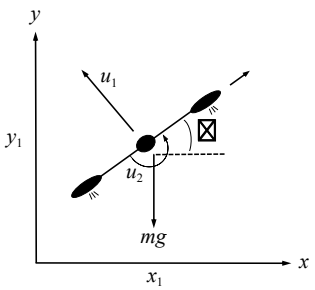

Fig. 1 VTOL model

elevation of the VTOL and the rolling moment of its corresponding center of mass, τ is the coupling between the rolling moment and the lateral acceleration; a minimal parameter which is usually neglected in the literature. To consider real-life applications, the system is subjected to parametric uncertainties and additive environmental external disturbances expressed by unknown terms $\psi_1(t)$ and $\psi_2(t)$. Although the values of the terms mentioned above are inherently uncertain, the upper bounds are assumed to be known as Assumption 1.

Assumption 1. The additive uncertainties and external disturbances $\psi_1(t)$ and $\psi_2(t)$ satisfy the following conditions:

$$\left|\psi_i(t)\right| \leq \rho_i\left(x, \dot{x}, y, \dot{y}\right) + l_i, \quad i = 1, 2 \tag{7}$$

where ρ_i is a positive term and l_i is a non-negative number. The VTOL UAV regulation problem consists of designing a robust controller such that the control laws u_1 and u_2 guarantee asymptotic convergence of $x(t) \to x_d(t)$ and $y(t) \to y_d(t)$ such that

$$\lim_{x \to \infty} \left\| \begin{pmatrix} y - y_d & x - x_d & \theta \end{pmatrix} \right\| = 0. \tag{8}$$

Accordingly, new state variables can be expressed as follows:

$$J = (J_1, J_2, J_3, J_4) = \left(x - x_d, \dot{x} - \dot{x}_d, y - y_d, \dot{y} - \dot{y}_d\right). \tag{9}$$

Rewriting (6) in the new coordinate system yields

$$\begin{aligned} \dot{J}_1 &= J_2 \\ \dot{J}_2 &= -u_1 \sin\theta + \tau u_2 \cos\theta - \ddot{x}_d + \psi_1 \\ \dot{J}_3 &= J_4 \\ \dot{J}_4 &= u_1 \cos\theta + \tau u_2 \sin\theta - \ddot{y}_d - 1 + \psi_2. \end{aligned} \tag{10}$$

Assumption 2. The angle $\theta(t) \in I_0$ holds for all the time, meaning that the acrobatic behavior is not possible.

2.3 Dynamic sliding mode control

Consider the following nonlinear system:

$$\begin{aligned} \dot{x} &= f(x, u) \\ y &= h(x, u) \end{aligned} \tag{11}$$

where $u \in \mathbf{R}^m$, $x \in \mathbf{R}^n$ and $y \in \mathbf{R}^m$ denote the system inputs, states and outputs vectors, respectively. $f(x, u)$ and $h(x, u)$ are nonlinear differentiable functions. The input-output model can be expressed as

$$y_i^{(n_i)} = \phi_i\left(\widehat{\boldsymbol{y}}, \widehat{\boldsymbol{u}}, t\right) + \psi_i, i = 1, 2, \cdots, m \tag{12}$$

where $\widehat{\boldsymbol{u}} = \left(u_1, \cdots, u_1^{(\beta_1)}, \cdots, u_m, \cdots, u_m^{(\beta_m)}\right)$, n_i is the integer derivative order, $\widehat{\boldsymbol{y}} = (y_1, \cdots, y_1^{(n_1-1)}, \cdots, y_m, \cdots,$

$y_m^{(n_m-1)}$), while $\beta_j, j=1,\cdots,m$ is the derivative order of input vector components. Considering known values $\rho_i>0$ and $l_i\geq 0$, the upper bond of additive uncertainties ψ_i can be expressed as follows:

$$|\psi_i|\leq \rho_i\|\widehat{\boldsymbol{y}}\|+l_i, i=1,\cdots,m \tag{13}$$

where

$$\begin{aligned}\rho^{(0)}&=\left[\sum_{i=1}^{m}\rho_i^2\right]^{\frac{1}{2}}\\ \rho^{(1)}&=\left[\sum_{i=1}^{m}\rho_i^2\right]^{\frac{1}{2}}\left(1+\max\left\{a_j^{(i)}\right\}\max\left\{\sqrt{n_i-1}\right\}\right)\\ \rho&=\rho^{(0)}+\rho^{(1)}/\left(4\theta_1\right)\end{aligned} \tag{14}$$

where $\theta_1\in(0,1)$ is a constant parameter and θ_0 is selected so that $\theta_0+\theta_1=1$.

Definition 1. The input-output model (12) with $\psi_i=0$ is proper if both input and output vectors have the same dimensions[32], and for $\widehat{\boldsymbol{y}}\in N_\delta(0)=\{J|J\in\mathbf{R}^n, J<\delta\}$ and $t\geq 0$, the following inequality is satisfied:

$$\det\left[\frac{\partial\left(\varphi_1,\cdots,\varphi_m\right)}{\partial\left(u^{(\beta_1)},\cdots,u^{(\beta_m)}\right)}\right]\neq 0. \tag{15}$$

Definition 2. The related zero dynamics for $\psi_i=0, i=1,\cdots,m$ to the input-output model (12) are defined as follows[36]:

$$\phi_i\left(0,\widehat{\boldsymbol{u}},t\right)=0, i=1,2,\cdots,m. \tag{16}$$

System (12) is minimum phase if and only if $\widehat{\boldsymbol{u}}_0\in\mathbf{R}^\beta$ and $\delta>0$, where $\beta=\beta_1+\cdots+\beta_m$. As a result, (16) is globally asymptotically stable with the initial condition $\widehat{\boldsymbol{u}}\left(0\right)\in N_\delta\left(\widehat{\boldsymbol{u}}_{\boldsymbol{0}}\right)$, where $\widehat{\boldsymbol{u}}=(u_1,\cdots,u_1^{(\beta_1-1)},\cdots,u_m,\cdots,u_m^{(\beta_m-1)})$. In order to simplify the design procedure, the following generalized canonical representation of (12) can be expressed.

$$\begin{cases}\dot{J}_1^{(1)}=J_2^{(1)}\\ \vdots\\ \dot{J}_{n_1-1}^{(1)}=J_{n_1}^{(1)}\\ \dot{J}_{n_1}^{(1)}=\varphi_1\left(J,\widehat{\boldsymbol{u}},t\right)+\psi_1\\ \vdots\\ \dot{J}_1^{(m)}=J_2^{(m)}\\ \vdots\\ \dot{J}_{n_{m-1}}^{(m)}=J_{n_m}^{(m)}\\ \dot{J}_{n_m}^{(m)}=\varphi_m\left(J,\widehat{\boldsymbol{u}},t\right)+\psi_m\end{cases} \tag{17}$$

where $J^{(i)}=(J_1^{(i)},\cdots,J_{n1}^{(i)})=(y_i,\cdots,y_i^{(n_i-1)}), i=1,\cdots,m$ and $J=\left(J^{(1)},\cdots,J^{(m)}\right)^{\mathrm{T}}$.

Unlike classical SMC, for which the sliding surface is defined based on state variables, in DSMC, it is defined according to the output and its derivatives. Matrices A_i and D_i are defined as follows:

$$\begin{aligned}A_i&=\begin{bmatrix}0&1&0&0&\cdots&0\\0&0&1&0&\cdots&0\\0&0&0&1&\cdots&\vdots\\\vdots&\vdots&\vdots&\ddots&\ddots&0\\0&0&0&0&0&1\\-a_1^{(i)}&-a_2^{(i)}&-a_3^{(i)}&-a_4^{(i)}&\cdots&-a_{n-1}^{(i)}\end{bmatrix}\\ D_i&=\begin{bmatrix}0&0&\cdots&0&1\end{bmatrix}^{\mathrm{T}}.\end{aligned} \tag{18}$$

Since A_i is Hurwitz, A is Hurwitz; thus A and P satisfy the Lyapunov equation $A^{\mathrm{T}}P+AP=-I_2$, where P is a positive definite matrix. By determining P and considering (12), K is obtained such that satisfies the following condition:

$$\lambda_{\min}\left(K\right)-\left[\frac{1}{\theta_0}(PD)^{\mathrm{T}}\left(PD\right)+\rho I_2\right]>0 \tag{19}$$

where $\lambda_{\min}(K)$ represents the smallest eigenvalue of K, and $I_2\in\mathbf{R}^{m\times m}$ is a unit vector. The sliding surface is then considered as

$$s_i=\sum_{j=1}^{n_i+1}a_j^{(i)}J_j^{(i)}+\phi_i\left(J,\widehat{\boldsymbol{u}},t\right),\quad i=1,\cdots,m \tag{20}$$

where $a_j^{(i)}$ is selected so that the polynomial $\sum_{j=1}^{n_i+1}a_j^{(i)}\lambda^{(j-1)}, i=1,\cdots,m$ is Hurwitz. In this work, the DSMC is designed considering the following reachability condition.

$$\dot{s}=-\gamma\left(\kappa,s\right) \tag{21}$$

where $s=[s_1,\cdots,s_m]$, and $\kappa=[\kappa_1,\cdots,\kappa_l]$ denotes the constant design parameters. Furthermore, $\gamma(\kappa,s)=[\gamma_1(\kappa,s),\cdots,\gamma_m(\kappa,s)]$ satisfies the following conditions: (a) $\gamma(\kappa,0)=0$, (b) $\gamma_i(\kappa,s)|_{i=1,\cdots,m}$ for $s_i\neq 0$ is a continuous function, and there exists a positive definite matrix K such that $s^{\mathrm{T}}\gamma(\kappa,s)>s^{\mathrm{T}}Ks$ for $s_i\neq 0$. Thus, the realization condition can be expressed as

$$\gamma_i(\kappa,s)=(K,s)_i+k_{0i}sat_\epsilon(s_i),\quad i=1,\cdots,m \tag{22}$$

where $(Ks)_i$ is the i-th component of Ks vector, and $K_0=\mathrm{diag}\left[k_{01},k_{0m}\right]\in\mathbf{R}^{m\times m}$. Considering the establishment of (21), (22) will satisfy the reaching law for all sliding surfaces. The derivative of (20) with respect to time is given by

$$\dot{s}_i = \sum_{j=1}^{n_i-1} a_j^{(i)} J_{j+1}^{(i)} + \phi_i\left(J, \widehat{\boldsymbol{u}}, t\right) + \psi_i\left(t\right), \quad i = 1, \cdots, m. \tag{23}$$

Thus, the control law must be designed such that it satisfies the following equation:

$$\sum_{j=1}^{n_i-1} a_j^{(i)} J_{j+1}^{(i)} + \phi_i\left(J, \widehat{\boldsymbol{u}}, t\right) + \psi_i\left(t\right) = -\left(Ks\right)_i - k_{0i} sat_\epsilon\left(s_i\right), \quad i = 1, \cdots, m. \tag{24}$$

Also, $sat_\varepsilon\left(s_i\right) = \left[sat_\varepsilon\left(s_1\right), \cdots, sat_\varepsilon\left(s_m\right)\right]^{\mathrm{T}}$ and $k_{0i} > l_0 = \left(\sum_{i=1}^{m} l_i^2\right)^{\frac{1}{2}}$, where $sat_\varepsilon(s_i)$ is defined as follows:

$$sat_\varepsilon\left(s_i\right) = \varepsilon sat\left(\frac{s_i}{\varepsilon}\right) = \begin{cases} 1, & \text{if } s_i > \varepsilon \\ \dfrac{s_i}{\varepsilon}, & \text{if } |s_i| \le \varepsilon \\ -1, & \text{if } s_i < -\varepsilon. \end{cases} \tag{25}$$

Considering (24), (21) can be rewritten as

$$\dot{s} = -\left(Ks\right)_i - K_0 sat_\varepsilon\left(s_i\right) + \psi\left(J, t\right). \tag{26}$$

3 Optimal HOB-DSMC design for VTOL UAV

3.1 Optimal HOB-DSMC controller

In this section, assuming that the state variables (J_2, J_4) are unmeasured, the proposed optimal HOB-DSMC approach is presented to deal with the trajectory tracking problem of the VTOL UAV system (12) subjected to additive uncertainties and external disturbances. The HSMO utilized to estimate the unmeasured variables (J_2, J_4) as well as disturbances (ψ_1, ψ_2) is given as

$$\begin{aligned}
\widehat{\dot{J}}_1 &= \widehat{J}_2 + \Omega_1 \left|\widetilde{J}_1\right|^{\frac{2}{3}} \mathrm{sgn}\left(\widetilde{J}_1\right) \\
\widehat{\dot{J}}_2 &= \Omega_2 \left|\widetilde{J}_1\right|^{\frac{1}{3}} \mathrm{sgn}\left(\widetilde{J}_1\right) - u_1 \sin\theta + \\
&\quad \tau u_2 \cos\theta + \psi_1\left(J, t\right) \\
\widehat{\dot{J}}_3 &= \widehat{J}_4 + \Omega_3 \left|\widetilde{J}_3\right|^{\frac{2}{3}} \mathrm{sgn}\left(\widetilde{J}_3\right) \\
\widehat{\dot{J}}_4 &= \Omega_4 \left|\widetilde{J}_3\right|^{\frac{1}{3}} \mathrm{sgn}\left(\widetilde{J}_3\right) + u_1 \cos\theta + \\
&\quad \tau u_2 \sin\theta - 1 + \psi_2\left(J, t\right) \\
\widehat{\dot{J}}_5 &= \Omega_5 \mathrm{sgn}\left(\widetilde{J}_1\right) \\
\widehat{\dot{J}}_6 &= \Omega_6 \mathrm{sgn}\left(\widetilde{J}_3\right)
\end{aligned} \tag{27}$$

where $\widehat{J}_i, i = 1, 2, \cdots, 6$ denote the estimated variables. Accordingly, the estimation errors can be expressed as $\widetilde{J}_i = J_i - \widehat{J}_i, i = 1, \cdots, 4$, $\widetilde{J}_5 = -\widehat{J}_5 + \psi_1$, and $\widetilde{J}_6 = -\widehat{J}_6 + \psi_2$. Similar definitions have been used in [37, 38]. Considering (10) and (27), the estimation error dynamics yield

$$\begin{aligned}
\dot{\widetilde{J}}_1 &= -\Omega_1 \left|\widetilde{J}_1\right|^{\frac{2}{3}} \mathrm{sgn}\left(\widetilde{J}_1\right) + \widetilde{J}_2 \\
\dot{\widetilde{J}}_2 &= -\Omega_2 \left|\widetilde{J}_1\right|^{\frac{1}{3}} \mathrm{sgn}\left(\widetilde{J}_1\right) + \widetilde{J}_5 \\
\dot{\widetilde{J}}_3 &= -\Omega_3 \left|\widetilde{J}_3\right|^{\frac{1}{3}} \mathrm{sgn}\left(\widetilde{J}_3\right) + \widetilde{J}_4 \\
\dot{\widetilde{J}}_4 &= -\Omega_4 \left|\widetilde{J}_3\right|^{\frac{1}{3}} \mathrm{sgn}\left(\widetilde{J}_3\right) + \widetilde{J}_6 \\
\dot{\widetilde{J}}_5 &= -\Omega_5 \mathrm{sgn}\left(\widetilde{J}_1\right) + \dot{\psi}_1 \\
\dot{\widetilde{J}}_6 &= \Omega_6 \mathrm{sgn}\left(\widetilde{J}_3\right) + \dot{\psi}_2.
\end{aligned} \tag{28}$$

The above-mentioned estimation error dynamics (28) are presented in the form of the non-recursive exact robust differentiator presented in [39], where the convergence proofs of (28) are well-studied utilizing quadratic and strict Lyapunov function[40], geometric approaches[40], and homogeneity properties[41]. Accordingly, an appropriate definition of the gains $\{\Omega_1, \Omega_2, \cdots, \Omega_6\}$ will lead to finite-time convergence of estimation error dynamics to zero[39, 40].

The sliding surface $s = [s_1, s_2]$ is proposed as follows:

$$\begin{aligned}
s_1(t) &= a_1 J_1(t) + \widehat{J}_2(t) \\
s_2(t) &= a_2 J_3(t) + \widehat{J}_4(t)
\end{aligned} \tag{29}$$

where $\{a_1, a_2\} > 0$. The derivative of (29) with respect to time yields

$$\begin{aligned}
\dot{s}_1 =& a_1 J_2 + \Omega_2 \left|\widetilde{J}_1\right|^{\frac{1}{3}} \mathrm{sgn}\left(\widetilde{J}_1\right) - u_1 \sin\theta + \\
& \tau u_2 \cos\theta + \psi_1\left(J, t\right) \\
\dot{s}_2 =& a_2 J_4 + \Omega_4 \left|\widetilde{J}_3\right|^{\frac{1}{3}} \mathrm{sgn}\left(\widetilde{J}_3\right) + u_1 \cos\theta + \\
& \tau u_2 \sin\theta - 1 + \psi_2\left(J, t\right).
\end{aligned} \tag{30}$$

Applying the reaching law conditions yields

$$\begin{aligned}
a_1 J_2 + \Omega_2 \left|\widetilde{J}_1\right|^{\frac{1}{3}} \mathrm{sgn}\left(\widetilde{J}_1\right) - u_1 \sin\theta + \tau u_2 \cos\theta + \\
\psi_1\left(J, t\right) = -\omega_{11} s_1 - \omega_{12} s_2 - k_{01} sat_\varepsilon\left(s_1\right) \\
a_2 J_4 + \Omega_4 \left|\widetilde{J}_3\right|^{\frac{1}{3}} \mathrm{sgn}\left(\widetilde{J}_3\right) + u_1 \cos\theta + \tau u_2 \sin\theta - \\
1 + \psi_2\left(J, t\right) = -\omega_{21} s_1 - \omega_{22} s_2 - k_{02} sat_\varepsilon\left(s_2\right)
\end{aligned} \tag{31}$$

where ω_{ij} is positive definite, $k_{0i} > I_0$, and in the sliding

reachability condition $\gamma_0(\kappa, s) = Ks$. The control laws are obtained as

$$
\begin{aligned}
u_1 = & -\frac{1}{\sin\theta\left(1+\cot^2\theta\right)}\times \\
& \Bigg[-\omega_{11}s_1 - \omega_{12}s_2 - k_{01}sat_\varepsilon(s_1) - a_1J_2 - \\
& \Omega_2\left|\widetilde{J}_1\right|^{1/3}\mathrm{sgn}\left(\widetilde{J}_1\right) + \\
& \cot\theta\Bigg(+\omega_{21}s_1 + \omega_{22}s_2 + k_{02}sat_\varepsilon(s_2) + \\
& a_2J_4 - \Omega_4\left|\widetilde{J}_3\right|^{1/3}\mathrm{sgn}\left(\widetilde{J}_3\right) - 1\Bigg)\Bigg] \\
u_2 = & -\frac{1}{\sin\theta\left(1-\cot^2\theta\right)}\times \\
& \Bigg[-\omega_{21}s_1 - \omega_{22}s_2 - k_{02}sat_\varepsilon(s_2) - a_2J_4 - \\
& \Omega_4\left|\widetilde{J}_3\right|^{1/3}\mathrm{sgn}\left(\widetilde{J}_3\right) + \\
& \cot\theta\Bigg(+\omega_{11}s_1 + \omega_{12}s_2 + k_{01}sat_\varepsilon(s_1) \\
& + a_1J_2 - \Omega_2\left|\widetilde{J}_1\right|^{1/3}\mathrm{sgn}\left(\widetilde{J}_1\right)\Bigg) + 1\Bigg].
\end{aligned} \tag{32}
$$

The control laws stated in (32) along with (12) yield a closed-loop system with arbitrarily initial conditions. To overcome the difficulty caused by the non-minimum phase behaviour, a robust dynamic control law is applied to minimize the chattering phenomenon. Considering (10) and (29), the error value $e = |J_1| + |J_2| + |J_3| + |J_4| = \|J_1 + J_2 + J_3 + J_4\|$ can be used. If $e > e_0$, where $0 < e_0 < 1$ is a small positive user-defined value, the control laws (32) are applied. As the error value reaches $e \le e_0$, the second control is activated and exponentially reduces the control effort. Let $\sigma > 0$,

$$
(\dot{\eta}_1, \dot{\eta}_2) = \begin{cases} \begin{cases} \dot{\eta}_1 = -b_1\mathrm{sgn}(\eta_1) \\ \dot{\eta}_2 = 0 \end{cases}, \text{if } |\eta_1| > \sigma_1 \\ \begin{cases} \dot{\eta}_1 = \eta_2 \\ \dot{\eta}_2 = -b_2\eta_1 - b_3\eta_2 \end{cases}, \text{if } |\eta_1| \le \sigma_1 \end{cases} \tag{33}
$$

where $(\eta_1, \eta_2) = (\theta, \dot{\theta})$ and $\{b_1, b_2, b_3\} > 0$ are optimized using FOFA in order to achieve the minimum control effort.

3.2 Stability analysis

Consider (29) as a coordinate transformation $J = (J_1, J_2, J_3, J_4) \leftrightarrow (J_1, s_1, J_2, s_2)$. In order to analyze the closed-loop system stability, it is essential to have an estimation of the uncertainty bounds in the $\left(\widetilde{J}, s\right)$ coordinate. The additive uncertainties and external disturbances expressed by (7) can be written in the $\left(\widetilde{J}, s\right)$ coordinate as follows:

$$
\|\psi_i(J,t)\| \le \rho_i\|J\| + l_i, \quad i = 1, 2. \tag{34}
$$

This leads to the estimate

$$
\|\psi(J,t)\| \le \rho^{(0)}\|J\| + l_0. \tag{35}
$$

where $\rho^{(0)} = \left(\rho_1^2 + \rho_2^2\right)^{\frac{1}{2}}$, $l_0 = \left(l_1^2 + l_2^2\right)^{\frac{1}{2}}$. Also

$$
\begin{aligned}
\|J\| \le & \left\|\widetilde{J}\right\| + \left((s_1 + a_1J_1)^2 + (s_2 + a_2J_3)^2\right)^{\frac{1}{2}} \le \\
& \left\|\widetilde{J}\right\| + \|s\| + \left((a_1J_1)^2 + (a_2J_3)^2\right)^{\frac{1}{2}} \le \\
& \left\|\widetilde{J}\right\| + \|s\| + \max\{a_1, a_2\}\left\|\widetilde{J}\right\|.
\end{aligned} \tag{36}
$$

Thus,

$$
\|\psi(J,t)\| = \left\|\psi\left(\widetilde{J}, s, t\right)\right\| \le \rho^{(1)}\left\|\widetilde{J}\right\| + \rho^{(0)}\|s\| + l_0 \tag{37}
$$

where $\rho^{(1)} = \rho^{(0)}(1 + \max\{a_1, a_2\})$. This yields the parameters stated in (14). It is also worth mentioning that the control law u_1 in (32) is static and bounded as long as $\left(\widetilde{J}, s\right)$ is bounded. In order to investigate the stability of the $\left(\widetilde{J}, s\right)$ dynamics, consider the following system:

$$
\begin{aligned}
\dot{\widetilde{J}} &= A\widetilde{J} + Ds \\
\dot{s} &= -\gamma_0(\kappa, s) - K_0sat_\varepsilon(s) + \psi(J,t).
\end{aligned} \tag{38}
$$

Suppose $s^{\mathrm{T}}\gamma_0(\kappa, s) \ge s^{\mathrm{T}}Ks$, where K satisfies

$$
\lambda_{\min}(K)\, I_2 - \left[\frac{1}{\theta_0}(PD)^{\mathrm{T}}(PD) + \rho I_2\right] > 0 \tag{39}
$$

where $K_0 > l_0I_2$. For arbitrary $\varepsilon_0 > 0$, the parameter ε in (25) can be chosen such that (38) is uniformly ultimately bounded by ε_0. The following Lyapunov function candidate is suggested:

$$
V = P\widetilde{J} + \frac{1}{2}s^{\mathrm{T}}s. \tag{40}
$$

Differentiating (40) along with the trajectories of (38) and using (37) yields

$$
\begin{aligned}
\dot{V} = & -\left\|\widetilde{J}\right\|^2 + 2\widetilde{J}^{\mathrm{T}}PDs - s^{\mathrm{T}}\gamma_0(\kappa, s) - \\
& s^{\mathrm{T}}k_0sat_\varepsilon(s) + s^{\mathrm{T}}\psi\left(\widetilde{J}, s, t\right) \le \\
& -\left\|\widetilde{J}\right\|^2 + 2\widetilde{J}^{\mathrm{T}}PDs - s^{\mathrm{T}}Ks - s^{\mathrm{T}}k_0sat_\varepsilon(s) + \\
& \|s\|\left(\rho^{(1)}\left\|\widetilde{J}\right\| + \rho^{(0)}\|s\| + l_0\right).
\end{aligned} \tag{41}
$$

Considering $\mathrm{sgn}(s) = [\mathrm{sgn}(s_1), \mathrm{sgn}(s_2)]^{\mathrm{T}}$ and using (42) and (43), (44) is obtained.

$$\rho^{(1)} \left\| \widetilde{J} \right\| \|s\| \leq \theta \left\| \widetilde{J} \right\|^2 + \frac{\left(\rho^{(1)}\right)^2}{4\theta} \|s\|^2 \tag{42}$$

$$\|s\| \leq |s_1| + |s_2| = s^{\mathrm{T}} \mathrm{sgn}(s) \tag{43}$$

$$\begin{aligned} \dot{V} =& -\left\| \widetilde{J} \right\|^2 + 2\widetilde{J}^{\mathrm{T}} PDs - s^{\mathrm{T}} \left(\lambda_{\min}(K)\right) I_2 s - s^{\mathrm{T}} k_0 sat_{\varepsilon}(s) + \\ & \left[\theta \left\| \widetilde{J} \right\|^2 + \left(\frac{\left(\rho^{(1)}\right)^2}{4\theta} + \rho^{(0)} \right) \|s\|^2 + s^{\mathrm{T}} (l_0 I) \mathrm{sgn}(s) \right] = \\ & \left[\widetilde{J}^{\mathrm{T}}, s^{\mathrm{T}} \right] \begin{bmatrix} -\theta_0 I_2 & [PD] \\ [PD]^{\mathrm{T}} & -\left(\left(\lambda_{\min}(K) - \rho\right) I_2\right) \end{bmatrix} \begin{bmatrix} \widetilde{J} \\ s \end{bmatrix} - \\ & \left(\sum_{\mu} \left(k_{0_\mu} - l_0\right) |s_\mu| + \sum_{\chi} \left(\frac{|s_\chi|}{\varepsilon} k_{0_\chi} - l_0 \right) |s_\chi| \right) \end{aligned} \tag{44}$$

where $\theta_0 = 1 - \theta$, μ and χ are subscripts where $|s_\mu| \geq \varepsilon$ and $|s_\chi| < \varepsilon$, respectively. Thus, suppose K satisfing:

$$\begin{aligned} \Gamma = & \begin{bmatrix} -\theta_0 I_{n-m} & -[PD] \\ -[PD]^{\mathrm{T}} & \left(\left(\lambda_{\min}(K) - \rho\right) I_2\right) \end{bmatrix} > 0 \\ & \lambda_{\min}(K) - \rho > 0. \end{aligned} \tag{45}$$

If all the s_i satisfy $|s_i| > \varepsilon$, then

$$\dot{V} \leq -\varphi_0 \left(\|\widetilde{J}\|^2 + \|s\|^2 \right) < 0, \left(\widetilde{J}, s\right) \neq 0 \tag{46}$$

where

$$\phi_0 = \min\left\{ \lambda_{\min}(\Gamma), \left(\lambda_{\min}(K), \rho\right), \lambda_{\min}(K_0 - l_0 I_2) \right\}. \tag{47}$$

Otherwise,

$$\begin{aligned} \dot{V} \leq & -\lambda_{\min}(K) \left(\|\widetilde{J}\|^2 + \|s\|^2 \right) - \sum_{\mu} \left(k_{0_\mu} - l_0\right) |s_\mu| - \\ & \sum_{\chi} \left(\frac{|s_\chi|}{\epsilon} k_{0_\chi} - l_0 \right) |s_\chi| \leq \\ & -\varphi_0 \|\widetilde{J}, s\|^2 + \sum_{\tau} |s_\tau| l_0 \leq \\ & -\varphi_0 \|\widetilde{J}, s\|^2 + 2 l_0 \epsilon < 0, \|\widetilde{J}, s\| > \sqrt{\frac{2 l_0 \epsilon}{\varphi_0}}. \end{aligned} \tag{48}$$

Thus, choosing $\varepsilon = \varepsilon_0^2 \phi_0 / 2 l_0$, system (38) is ultimately bounded by $\varepsilon_0 = (2 l_0 \varepsilon / \phi_0)^{\frac{1}{2}}$ if (45) is satisfied. Since the Lyapunov function candidate V is radially bounded, (38) is globally uniformly ultimately bounded by ε_0 if (45) is satisfied.

4 Simulation results

In this section, simulation results for two maneuvers are illustrated to testify the proposed optimal HOB-DSMC control scheme's performance for VTOL UAV trajectory tracking. The first maneuver is dedicated to performance verification of the proposed control scheme, with different reference trajectories, while the second maneuver validates the performance of the proposed control scheme in comparison with conventional SMC and integral SMC (ISMC)[42] approaches. It is worth mentioning that the VTOL is assumed to move in the XY plane. Thus, the height and the yaw angle of the VTOL are not involved in the trajectory tracking and specified to be constants; however, they can be controlled separately.

4.1 Performance verification

In this maneuver, the closed-loop system consisting of the VTOL model presented in (6) and the proposed optimal HOB-DSMC control scheme is required to track various reference trajectories in the presence of external disturbances $\psi_1(t)$ and $\psi_2(t)$. Three reference trajectories are considered in this maneuver: (a) circle, (b) reverse spiral circle, and (c) 8-shape. The parameters settings for the controller and optimization algorithm are listed in Tables 1 and 2, respectively.

The achieved results are illustrated in Fig. 2, where it can be considered as a well-suited performance index to

Table 1 Proposed controller parameters

Parameter	Value	Parameter	Value
ω_{11}	6.5	τ	0.01
ω_{12}	0.5	a_1	3
ω_{21}	0.5	a_2	4
ω_{22}	6.5	b_1	9
k_{01}	1.5	b_2	6.8
k_{02}	1.5	b_3	7.3

Table 2 Fractional-order firefly algorithm parameter settings

Parameter	Value
Fractional order	$\Omega = 0.7$
Number of population	50
Max of iteration	50
Light absorption	$\gamma = 0.9$
Attractiveness at $r = 0$	$\beta_0 = 1.8$
Mutation coefficient	$\alpha = 0.25$

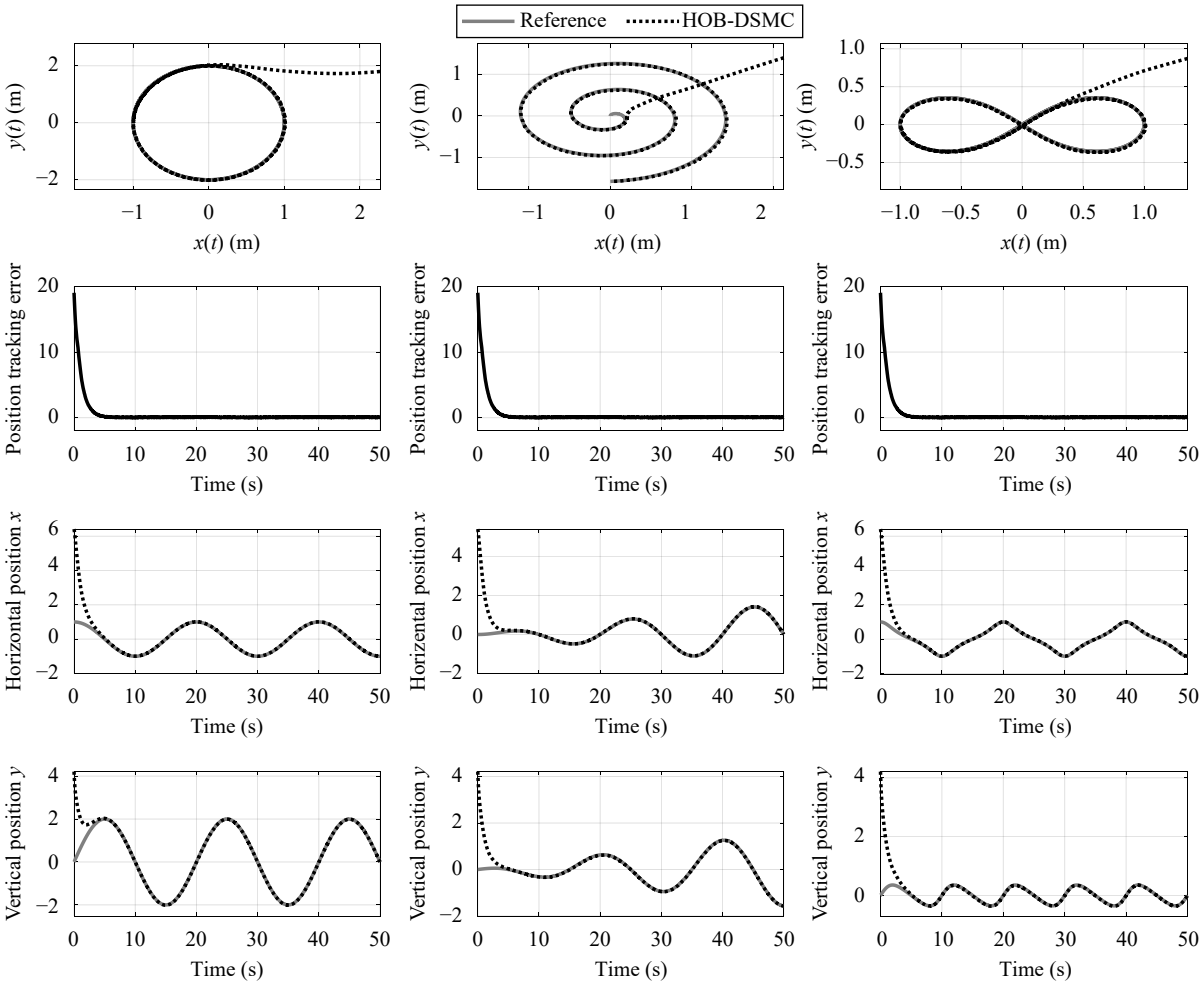

Fig. 2 Closed-loop system trajectory tracking responses using optimal HOB-DSMC

investigate the performance of the proposed control strategy in the presence of external disturbances. According to Fig. 2, three following prescribed trajectories are considered: round, reverse spiral round, and 8-shaped trajectories. As it is observed, with respect to the reference trajectory, each position tracking error component asymptotically converges to almost zero in less than 5 s. Consequently, the simulation results demonstrated in Fig. 2 show that the proposed HOB-DSMC can effectively compensate for the effects of external disturbances, delivering asymptotically stable position errors, which demonstrates the accomplishment of the tracking mission.

4.2 Performance comparison

Comparative simulations are carried out in this maneuver to testify and highlight the performance of the proposed optimal DOB-DSMC controller. To this end, a reverse spiral 8-shape trajectory is considered as the reference, and the tracking performance of the proposed DOB-DSMC is evaluated compared to the conventional SMC and ISMC approaches. Simulation results are depicted in Figs. 3–8. Fig. 3 illustrates the reference trajectory tracking performance comparison of the control approaches under investigation. According to Fig. 3, all three approaches can track the reference trajectory with different performance levels. Compared to SMC and ISMC, it is readily observed that the optimized dynamic SMC augmented with the high-order observer accomplishes the trajectory tracking mission more precisely with less position tracking error, as shown in Fig. 4.

The comparative closed-loop horizontal and vertical position and velocity tracking responses are demonstrated in Figs. 5 and 6, respectively, where accordingly, the superior performance of optimal HOB-DSMC with respect to SMS and ISMC approaches is apparent. Figs. 7 and 8 illustrate comparisons of control inputs and sliding variables of SMC, ISMC, and HOB-DSMC approaches, respectively. As shown in Fig. 7, compared with SMC and ISMC, the proposed controller's oscillations are much lower. Furthermore, the markedly better convergence speed of sliding variables in HOB-DSMC is observed in Fig. 8, which demonstrates the superior performance of HOB-DSMC in comparison with SMC and ISMC.

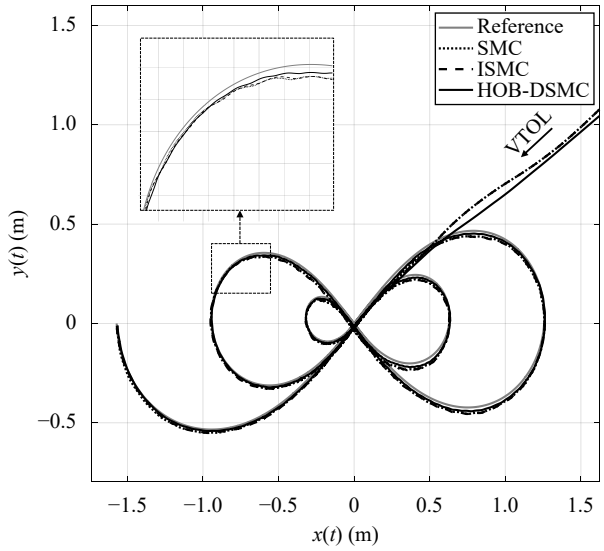

Fig. 3 Performance comparison of SMC, ISMC, and HOB-DSMC for reverse spiral 8-shape reference trajectory tracking

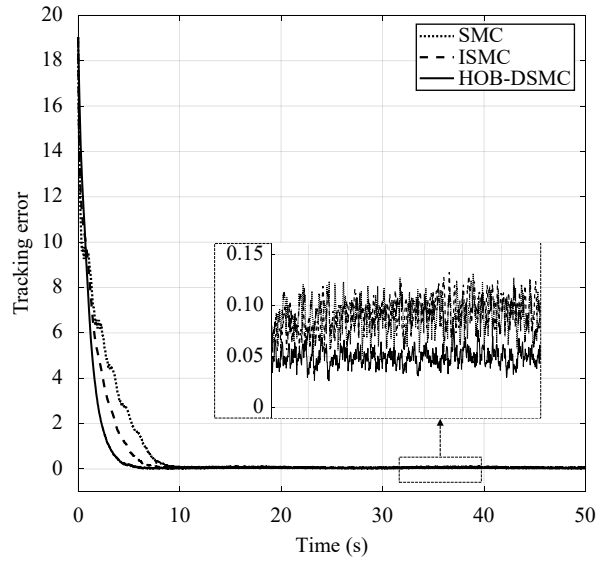

Fig. 4 Comparison of closed-loop position tracking errors

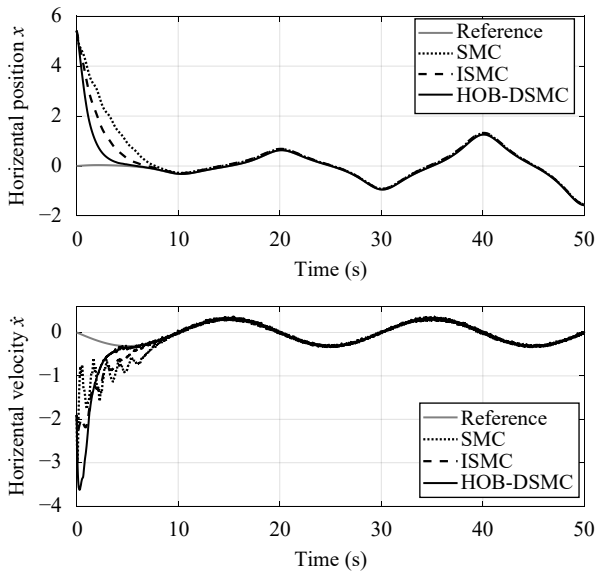

Fig. 5 Comparison of closed-loop horizontal position and velocity tracking responses

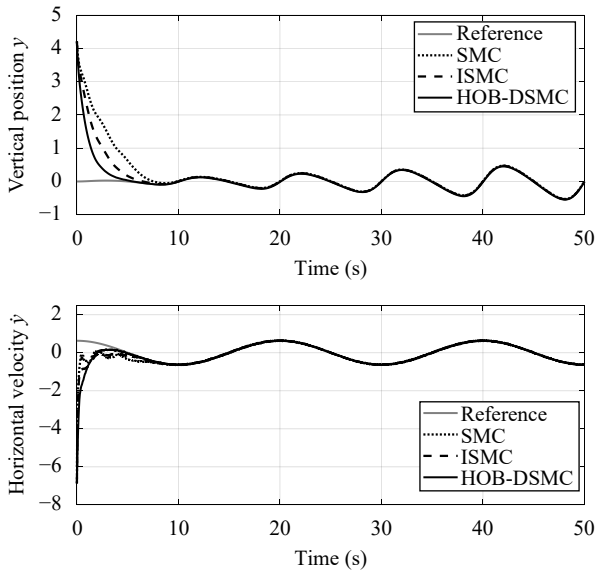

Fig. 6 Comparison of closed-loop vertical position and velocity tracking responses

According to the results achieved, it is observed that utilizing the higher-order sliding mode observer to estimate the unmeasured variables, taking advantage of the robust variable-structure control law and the optimization procedure has noticeably enhanced the controllers' performance.

5 Conclusions

This paper proposed a dynamic SMC scheme to deal with the unmanned aerial vehicles' trajectory tracking problem subjected to external disturbances. The proposed control scheme consists of a higher-order observer to estimate the unmeasured variables, alleviate the chattering phenomenon's effects, and a second control strategy to reduce the control input. In this regard, a neighboring point close to the sliding surface was considered as the error threshold for activating the second control, augmented with the fractional-order firefly algorithm to maintain the optimal controller parameters. In order to validate the performance of the proposed scheme, three reference trajectories were considered: circle, reverse spiral circle, and 8-shape. Furthermore, the efficiency of the proposed HOB-DSMC on the VTOL UAV model in the presence of external disturbances has been investigated compared to conventional SMC and in-

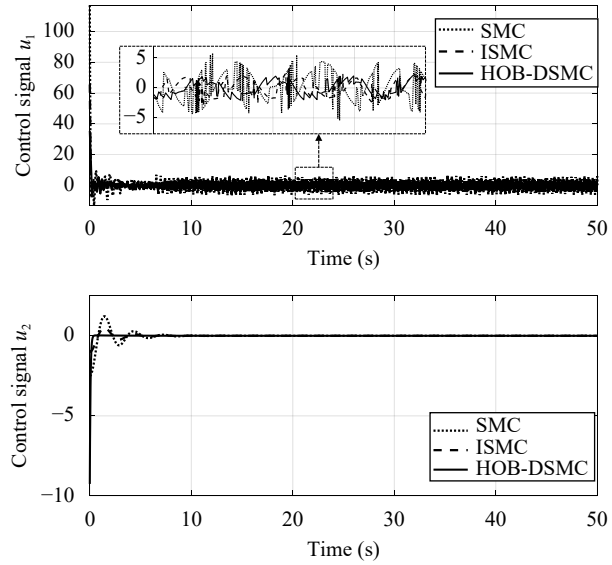

Fig. 7 Comparison of control inputs for SMC, ISMC and HOB-DSMC

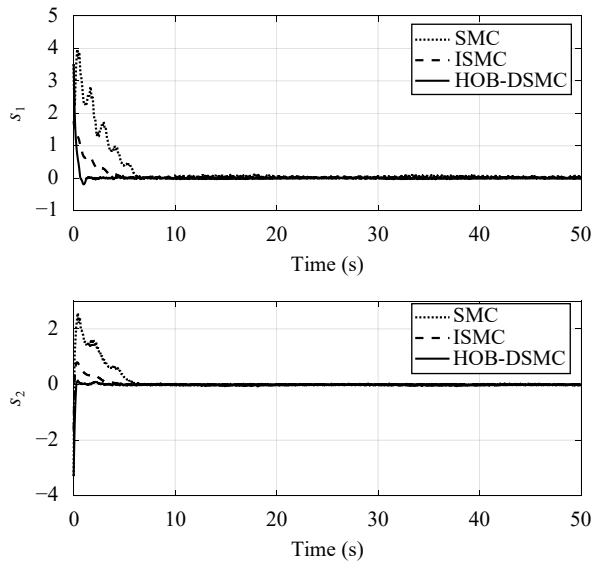

Fig. 8 Comparison of sliding variables for SMC, ISMC and HOB-DSMC

tegral SMC approaches, where the controller parameters were tuned using FOFA. Simulation results indicated the effectiveness of the proposed optimal HOB-DSMC scheme. Several future works can be explored according to the present study; for instance, the control procedure can be used for the image-based control used for obstacle avoidance, proposing new control schemes to stabilize a wide range of underactuated systems and experimental validations of the proposed approach.

References

[1] H. Bin, J. C. Wang. Deep learning based hand gesture recognition and OAV flight controls. *International Journal of Automation and Computing*, vol. 17, no. 1, pp. 27–29, 2020. DOI: 10.1007/s11633-019-1194-7.

[2] F. Zhou, W. Zheng, Z. F. Wang. Adaptive noise identification in vision-assisted motion estimation for unmanned aerial vehicles. *International Journal of Automation and Computing*, vol. 12, no. 4, pp. 413–420, 2015. DOI: 10.1007/s11633-014-0857-7.

[3] M. D. Hua, T. Hamel, P. Morin, C. Samson. A control approach for thrust-propelled underactuated vehicles and its application to VTOL drones. *IEEE Transactions on Automatic Control*, vol. 54, no. 8, pp. 1837–1853, 2009. DOI: 10.1109/TAC.2009.2024569.

[4] A. Arab, Y. Mousavi. Optimal control of wheeled mobile robots: From simulation to real world. In *Proceedings of American Control Conference*, IEEE, Denver, USA, pp. 583−589, 2020. DOI: 10.23919/ACC45564.2020.9147898.

[5] M. R. Cohen, J. R. Forbes. Navigation and control of unconventional VTOL UAVs in forward-flight with explicit wind velocity estimation. *IEEE Robotics and Automation Letters*, vol. 5, no. 2, pp. 1151–1158, 2020. DOI: 10.1109/LRA.2020.2966406.

[6] J. G. Romero, H. Rodriguez-Cortes. Asymptotic stability for a transformed nonlinear UAV model with a suspended load via energy shaping. *European Journal of Control*, vol. 52, pp. 87–96, 2020. DOI: 10.1016/j.ejcon.2019.09.002.

[7] M. D. Hua, T. Hamel, P. Morin, C. Samson. Introduction to feedback control of underactuated VTOLvehicles: A review of basic control design ideas and principles. *IEEE Control Systems Magazine*, vol. 33, no. 1, pp. 61–75, 2013. DOI: 10.1109/MCS.2012.2225931.

[8] R. Naldi, M. Furci, R. G. Sanfelice, L. Marconi. Robust global trajectory tracking for underactuated VTOL aerial vehicles using inner-outer loop control paradigms. *IEEE Transactions on Automatic Control*, vol. 62, no. 1, pp. 97–112, 2017. DOI: 10.1109/TAC.2016.2557967.

[9] B. B. Kocer, T. Tjahjowidodo, G. G. Lee Seet. Centralized predictive ceiling interaction control of quadrotor VTOL UAV. *Aerospace Science and Technology*, vol. 76, pp. 455–465, 2018. DOI: 10.1016/j.ast.2018.02.020.

[10] Y. Bouzid, H. Siguerdidjane, Y. Bestaoui. Nonlinear internal model control applied to VTOL multi-rotors UAV. *Mechatronics*, vol. 47, pp. 49–66, 2017. DOI: 10.1016/j.mechatronics.2017.08.002.

[11] Y. Zou, Z. Y. Coordinated trajectory tracking of multiple vertical take-off and landing UAVs. *Automatica*, vol. 99, pp. 33–40, 2019. DOI: 10.1016/j.automatica.2018.10.011.

[12] Y. Zou, Z. Y. Meng. Leader-follower formation control of multiple vertical takeoff and landing UAVs: Distributed estimator design and accurate trajectory tracking. In *Proceedings of the 13th IEEE International Conference on Control & Automation*, IEEE, Ohrid, Macedonia, pp. 764−769, 2017. DOI: 10.1109/ICCA.2017.8003156.

[13] A. Abdessameud, F. Janabi-Sharifi. Image-based tracking control of VTOL unmanned aerial vehicles. *Automatica*, vol. 53, pp. 111–119, 2015. DOI: 10.1016/j.automatica.2014.12.032.

[14] A. Abdessameud, F. Janabi-Sharifi. Dynamic image-based tracking control for VTOL UAVs. In *Proceedings of the 52nd IEEE Conference on Decision and Control*, IEEE, Firenze, Italy, pp. 7666−7671, 2013. DOI: 10.1109/CDC.2013.6761106.

[15] N. Guenard, T. Hamel, R. Mahony. A practical visual servo control for an unmanned aerial vehicle. *IEEE Transactions on Robotics*, vol. 24, no. 2, pp. 331–340, 2008. DOI: 10.1109/TRO.2008.916666.

[16] J. C. Escobar, R. Lozano, M. B. Estrada. PVTOL control using feedback linearisation with dynamic extension. *International Journal of Control*, 2019. DOI: 10.1080/00207179.2019.1676468.

[17] K. Wang, C. C. Hua, J. N. Chen, M. J. Cai. Dual-loop integral sliding mode control for robust trajectory tracking of a quadrotor. *International Journal of Systems Science*, vol. 51, no. 2, pp. 203–216, 2020. DOI: 10.1080/00207721.2019.1622815.

[18] C. Aguilar-Ibanez, M. S. Suarez-Castanon, J. Mendoza-Mendoza, J. de Jesus Rubio, J. C. Martinez-Garcia. Output-feedback stabilization of the pvtol aircraft system based on an exact differentiator. *Journal of Intelligent & Robotic Systems*, vol. 90, no. 3–4, pp. 443–454, 2018. DOI: 10.1007/s10846-017-0660-0.

[19] X. S. Yang. Firefly algorithm. *Engineering Optimization: An Introduction with Metaheuristic Applications*, X. S. Yang, Ed., Hoboken, USA: John Wiley & Sons, Inc., pp. 79–90, 2010. DOI: 10.1002/9780470640425.ch17.

[20] A. Banerjee, D. Ghosh, S. Das. Modified firefly algorithm for area estimation and tracking of fast expanding oil spills. *Applied Soft Computing*, vol. 73, pp. 829–847, 2018. DOI: 10.1016/j.asoc.2018.09.024.

[21] I. B. Aydilek. A hybrid firefly and particle swarm optimization algorithm for computationally expensive numerical problems. *Applied Soft Computing*, vol. 66, pp. 232–249, 2018. DOI: 10.1016/j.asoc.2018.02.025.

[22] F. Pazhoohesh, S. Hasanvand, Y. Mousavi. Optimal harmonic reduction approach for PWM AC–AC converter using nested memetic algorithm. *Soft Computing*, vol. 21, no. 10, pp. 2761–2776, 2017. DOI: 10.1007/s00500-015-1979-8.

[23] T. Niknam, R. Azizipanah-Abarghooee, A. Roosta. Reserve constrained dynamic economic dispatch: A new fast self-adaptive modified firefly algorithm. *IEEE Systems Journal*, vol. 6, no. 4, pp. 635–646, 2012. DOI: 10.1109/JSYST.2012.2189976.

[24] Y. Mousavi, A. Alfi. Fractional calculus-based firefly algorithm applied to parameter estimation of chaotic systems. *Chaos, Solitons & Fractals*, vol. 114, pp. 202–215, 2018. DOI: 10.1016/j.chaos.2018.07.004.

[25] Y. Mousavi, A. Alfi, I. B. Kucukdemiral. Enhanced fractional chaotic whale optimization algorithm for parameter identification of isolated wind-diesel power systems. *IEEE Access*, vol. 8, pp. 140862–140875, 2020. DOI: 10.1109/ACCESS.2020.3012686.

[26] Y. Mousavi, A. Alfi. A memetic algorithm applied to trajectory control by tuning of fractional order proportional-integral-derivative controllers. *Applied Soft Computing*, vol. 36, pp. 599–617, 2015. DOI: 10.1016/j.asoc.2015.08.009.

[27] G. W. Zhang, P. Yang, J. Wang, J. J. Sun, Y. Zhang. Integrated observer-based fixed-time control with backstepping method for exoskeleton robot. *International Journal of Automation and Computing*, vol. 17, no. 1, pp. 71–82, 2020. DOI: 10.1007/s11633-019-1201-z.

[28] M. Chavoshian, M. Taghizadeh, M. Mazare. Hybrid dynamic neural network and PID control of pneumatic artificial muscle using the PSO algorithm. *International Journal of Automation and Computing*, vol. 17, no. 3, pp. 428–438, 2020. DOI: 10.1007/s11633-019-1196-5.

[29] V. A. Le, H. X. Le, L. Nguyen, M. X. Phan. An efficient adaptive hierarchical sliding mode control strategy using neural networks for 3D overhead cranes. *International Journal of Automation and Computing*, vol. 16, no. 5, pp. 614–627, 2019. DOI: 10.1007/s11633-019-1174-y.

[30] I. Zaidi, M. Chtourou, M. Djemel. Robust neural control of discrete time uncertain nonlinear systems using sliding mode backpropagation training algorithm. *International Journal of Automation and Computing*, vol. 16, no. 2, pp. 213–225, 2019. DOI: 10.1007/s11633-017-1062-2.

[31] A. Nizar, B. M. Houda, N. A. Said. A new sliding function for discrete predictive sliding mode control of time delay systems. *International Journal of Automation and Computing*, vol. 10, no. 4, pp. 288–295, 2013. DOI: 10.1007/s11633-013-0723-z.

[32] A. H. D. Markazi, M. Maadani, S. H. Zabihifar, N. Doost-Mohammadi. Adaptive fuzzy sliding mode control of under-actuated nonlinear systems. *International Journal of Automation and Computing*, vol. 15, no. 3, pp. 364–376, 2018. DOI: 10.1007/s11633-017-1108-5.

[33] M. B. R. Neila, D. Tarak. Adaptive terminal sliding mode control for rigid robotic manipulators. *International Journal of Automation and Computing*, vol. 8, no. 2, pp. 215–220, 2011. DOI: 10.1007/s11633-011-0576-2.

[34] A. J. Koshkouei, K. J. Burnham, A. S. I. Zinober. Dynamic sliding mode control design. *IEE Proceedings – Control Theory and Applications*, vol. 152, no. 4, pp. 392–396, 2005. DOI: 10.1049/ip-cta:20055133.

[35] C. Aguilar-Ibanez, H. Sira-Ramirez, M. S. Suarez-Castanon, R. Garrido. Robust trajectory-tracking control of a PVTOL under crosswind. *Asian Journal of Control*, vol. 21, no. 3, pp. 1293–1306, 2019. DOI: 10.1002/asjc.1817.

[36] R. Olfati-Saber. Global configuration stabilization for the VTOL aircraft with strong input coupling. *IEEE Transactions on Automatic Control*, vol. 47, no. 11, pp. 1949–1952, 2002. DOI: 10.1109/TAC.2002.804457.

[37] A. Chalanga, S. Kamal, L. Fridman, B. Bandyopadhyay, J. A. Moreno. How to implement super-twisting controller based on sliding mode observer. In *Proceedings of the 13th International Workshop on Variable Structure Systems*, IEEE, Nantes, France, 2014. DOI: 10.1109/VSS.2014.6881145.

[38] A. Chalanga, S. Kamal, L. M. Fridman, B. Bandyopadhyay, J. A. Moreno. Implementation of super-twisting control: Super-twisting and higher order sliding-mode observer-based approaches. *IEEE Transactions on Industrial Electronics*, vol. 63, no. 6, pp. 3677–3685, 2016. DOI: 10.1109/TIE.2016.2523913.

[39] A. Levant. Higher-order sliding modes, differentiation and output-feedback control. *International Journal of Control*, vol. 76, no. 9–10, pp. 924–941, 2003. DOI: 10.1080/00207170310000099029.

[40] J. A. Moreno. Lyapunov function for levant's second order differentiator. In *Proceedings of the 51st IEEE Conference on Decision and Control*, IEEE, Maui, USA, pp. 6448–6453, 2012. DOI: 10.1109/CDC.2012.6426877.

[41] A. Levant. Homogeneity approach to high-order sliding mode design. *Automatica*, vol. 41, no. 5, pp. 823–830, 2005.

DOI: 10.1016/j.automatica.2004.11.029.

[42] Y. Guo, B. Huang, A. J. Li, C. Q. Wang. Integral sliding mode control for Euler-Lagrange systems with input saturation. *International Journal of Robust and Nonlinear Control*, vol. 29, no. 4, pp. 1088–1100, 2019. DOI: 10.1002/rnc.4431.

Yashar Mousavi received the M. Sc. degree in control engineering from Shahrood University of Technology, Iran in 2014. He is currently a Ph. D. degree candidate as a member of the Power and Renewable Energy Systems (PRES) Research Division with Department of Applied Science, School of Computing, Engineering and Built Environment, Glasgow Caledonian University, UK.

His research interests include evolutionary optimization, renewable energy, robotic systems and control, robust nonlinear control, fractional-order control, and fault-tolerant control.

E-mail: seyedyashar.mousavi@gcu.ac.uk (Corresponding author)
ORCID ID: 0000-0002-6718-3599

Amin Zarei received the B. Sc. degree in electrical engineering from University of Sistan and Baluchestan, Iran in 2011 and the M. Sc. degree in control engineering from Shahrood University of Technology, Iran in 2014. He is currently a Ph. D. degree candidate in control engineering at University of Sistan and Baluchestan, Iran.

His research interests include complex systems, networked control systems, nonlinear control, chaos theory, and time series prediction.

E-mail: amin.zarei@pgs.usb.ac.ir
ORCID ID: 0000-0003-2326-4431

Arash Mousavi received the B. Sc. degree in control engineering from Payam University, Iran in 2013, and the M. Sc. degree in electrical engineering from Islamic Azad University of Jahrom, Iran in 2016. He is currently the head of Electrical Engineering Research Lab (EERL) with Department Electrical Engineering and Applied Sciences, Paradise Research Center, Iran.

His research interests include renewable energy, robotic systems and control, power systems, impacts of distributed generations on power systems, and reliability of power systems.

E-mail: mousavii.arash@gmail.com

Mohsen Biari received the B. Sc. and the M. Sc. degrees in control engineering from Shahrood University of Technology, Iran in 2010 and 2013, respectively. He is currently the head of Robotics and Automation research Lab with Science and Technology Center, Iran.

His research interests include robotic systems and control, nonlinear control, fault-tolerant control, autonomous control, and computer vision.

E-mail: mohsen.biari@gmail.com

IJAC International Journal of Automation & Computing

Citation: Y. Mousavi, A. Zarei, A. Mousavi, M. Biari. Robust optimal higher–order–observer–based dynamic sliding mode control for vtol unmanned aerial vehicles. *International Journal of Automation and Computing*, vol.18, no.5, pp.802–813, 2021. https://doi.org/10.1007/s11633–021–1282–3